HOKKAIDO UNIVERSITY

Title	Radiation balance of the tropical tropopause layer
Author(s)	Gettelman, Andrew; Forster, Piers M. de F.; Masatomo, Fujiwara et al.
Citation	Journal of Geophysical Research Atmospheres, 109(D7), D07103 https://doi.org/10.1029/2003JD004190
Issue Date	2004-04-16
Doc URL	https://hdl.handle.net/2115/64834
Rights	Copyright 2004 American Geophysical Union.
Type	journal article
File Information	Gettelman_et_al-2004-Journal_of_Geophysical_Research__Atmospheres_(1984-2012).pdf

Hokkaido University Collection of Scholarly and Academic Papers : HUSCAP

Radiation balance of the tropical tropopause layer

Andrew Gettelman,[1] Piers M. de F. Forster,[2,3] Masatomo Fujiwara,[4] Qiang Fu,[5] Holger Vömel,[6] Laila K. Gohar,[2] Celeste Johanson,[5] and Marie Ammerman[5]

Received 26 September 2003; revised 5 February 2004; accepted 18 February 2004; published 8 April 2004.

[1] The radiation balance of the tropical tropopause layer (TTL) is examined using several different radiation codes with standard profiles compiled from observations in the tropics assuming clear sky conditions. These codes include detailed radiative transfer models and simplified codes for global climate models. The importance of the various radiatively active gases are examined. Water vapor is the most important contributor to the TTL radiation balance, but carbon dioxide and ozone also play a role. Differences in radiative heating between radiation models are mostly due to treatments of shortwave radiation. Differences between models below the TTL are due to different treatments of water vapor continuum absorption. The level of zero clear sky radiative heating, a level important for understanding the transport of air into the stratosphere, is generally found near 15 km, 125 hPa and 200°K (360 K potential temperature), consistent with previous work. Changes in time and space can modify this level by ±500 m, and individual profiles vary from these averages by ±400 m (1σ). Increases in water vapor in the TTL would tend to increase the altitude of the level at which the net heating is zero, while increases in carbon dioxide or ozone would tend to decrease this level. Clouds in the TTL tend to increase the level due to enhancements in longwave cooling above clouds. The implications for transport are discussed. *INDEX TERMS:* 3359 Meteorology and Atmospheric Dynamics: Radiative processes; 3362 Meteorology and Atmospheric Dynamics: Stratosphere/troposphere interactions; 3374 Meteorology and Atmospheric Dynamics: Tropical meteorology; *KEYWORDS:* radiation, tropical tropopause

Citation: Gettelman, A., P. M. de F. Forster, M. Fujiwara, Q. Fu, H. Vömel, L. K. Gohar, C. Johanson, and M. Ammerman (2004), Radiation balance of the tropical tropopause layer, *J. Geophys. Res.*, *109*, D07103, doi:10.1029/2003JD004190.

1. Introduction

[2] As recently noted by *Highwood and Hoskins* [1998], the tropical tropopause is less a material surface than a transition region between the troposphere and the stratosphere. The transition region around the tropopause is known as the Tropical Tropopause Layer (TTL), commonly defined as the layer extending vertically from the level of main convective outflow at 10–14 km to the cold point tropopause [*Gettelman and Forster*, 2002].

[3] The TTL contains the region in which most of the air enters the stratosphere [*Brewer*, 1949], but how air enters the stratosphere through the TTL is uncertain. Various processes are important for transporting air in the TTL and into the stratosphere. These processes include cumulus convection which overshoots its level of neutral buoyancy [*Sherwood*, 2000], large-scale waves [*Fujiwara et al.*, 2001], horizontal transport and slow diabatic ascent [*Holton and Gettelman*, 2001]. Because the water vapor concentration in the stratosphere appears to have increased over the last 20 years [*Oltmans et al.*, 2000] and that increase is not fully understood [*Stratospheric Processes and Their Role in Climate* (*SPARC*), 2000], understanding how air and water vapor enter the stratosphere are of critical importance.

[4] Air enters the TTL from the underlying troposphere largely through convection [*Folkins et al.*, 2000]. Convection dominates the lower portion of the TTL, but the frequency of convection declines rapidly with height [*Gettelman et al.*, 2002]. Outside of convective clouds, the radiative balance of the TTL determines the direction and magnitude of vertical motion. Vertical motion in the TTL, driven or balanced by radiative heating and cooling, is thus critical for understanding how air enters the stratosphere.

[5] Radiative heating in the TTL is a result of heating from the absorption of infrared radiation by ozone and carbon dioxide balanced by infrared cooling mostly from water vapor [*Thuburn and Craig*, 2002]. The level at which

[1]National Center for Atmospheric Research, Boulder, Colorado, USA.
[2]Department of Meteorology, University of Reading, Reading, UK.
[3]Also at Aeronomy Laboratory, National Oceanic and Atmospheric Administration, Boulder, Colorado, USA.
[4]Graduate School of Environmental Earth Science, Hokkaido University, Sapporo, Japan.
[5]Department of Atmospheric Sciences, University of Washington, Seattle, Washington, USA.
[6]Climate Monitoring and Diagnostics Laboratory, National Oceanic and Atmospheric Administration, Boulder, Colorado, USA.

Copyright 2004 by the American Geophysical Union.
0148-0227/04/2003JD004190

the background clear sky radiative heating rate (Q_{clear}) changes from a net cooling to a net heating occurs in the TTL [*Sherwood*, 2000; *Folkins et al.*, 2000]. This is the level to which a parcel must be lifted for the background atmospheric net radiative heating to lift it into the stratosphere. The level has been termed the 'stagnation surface' by *Sherwood and Dessler* [2003], and at this level residence times of trajectories in the TTL become long [*Fueglistaler et al.*, 2004].

[6] Several recent studies have reported the level of $Q_{clear} = 0$. *Folkins et al.* [1999] estimated that clear sky mass flux changes sign at 15 km, also stated as a potential temperature of 357 K [*Folkins et al.*, 2000]. For clarity in this study we will use '°K' to refer to temperature and 'K' to refer to potential temperature, both in Kelvins. *Sherwood* [2000] estimated the level at 135 hPa, or 14.8 km. *Gettelman and Forster* [2002] estimated the level of $Q_{clear} = 0$ as ~16 km, within ~1 km of the cold point tropopause. In addition, *Hartmann and Larson* [2002] have noted that the level of zero heating is at a temperature of ~200°K and is coupled to the water vapor distribution, because as the amount of water vapor decreases with temperature, the net cooling decreases.

[7] In this paper, we seek a better understanding of the variability and components of the radiative balance to better characterize the transport of air in the TTL. We seek to understand how diabatic heating varies and how radiative heating is affected by changes to radiatively active species and clouds.

[8] The methodology and details regarding the data and the various radiation models used are presented in Section 2. Detailed results are presented in Section 3. In Section 4 we examine these results in context of the transport of air in the TTL and the interaction between the radiation balance and clouds. Conclusions are given in Section 5.

2. Methodology

[9] To better understand the radiation balance of the TTL and how it affects transport, we will use a suite of column radiation models and observed atmospheric profiles. We will examine the factors that control the net radiative balance of the TTL, and that affect the entry of air into the stratosphere. In particular, we wish to understand where the net heating is positive (air is rising) or negative (air is sinking). As a convenient diagnostic, we will use the level of zero net radiative heating $Q_{clear} = 0$. Above this level air is rising into the stratosphere, and below this level air is sinking into the troposphere.

[10] Key questions to examine include: What are the contributions from various radiatively active greenhouse gases? What is the variability in the radiation balance to changes in input profiles? What is the effect of clouds? What are the uncertainties based on differences between radiation codes, especially those for global climate models versus detailed codes?

[11] We use four different radiation models in this study, and compare them using identical input parameters as much as possible. After examining the input data, we look at the radiation balance and the impact of the various radiatively active gases in the longwave and shortwave. We will intercompare the models, and look at the level of $Q_{clear} = 0$ in some detail. Finally, we examine the sensitivity of this level to changes in greenhouse gases and clouds.

2.1. Data

[12] For this study 5 standard atmospheric profiles were derived from various data. To obtain consistent profiles of temperature, water vapor and ozone through the TTL at high vertical resolution, balloon observations were used. Simultaneous observations of temperature, ozone and water vapor are derived from tropical balloon soundings [*Vömel et al.*, 2002]. Temperatures are taken from a standard radiosonde sensor. Water vapor profiles were measured with a Vaisala radiosonde Humidicap sensor and a National Oceanic and Atmospheric Administration Climate Monitoring and Diagnostics Laboratory (NOAA/CMDL) frost point hygrometer. A more detailed description and validation of the ozone data is described by *Thompson et al.* [2003a]. These observations were averaged to develop a set of seasonal climatologies. Five profiles were derived: from the eastern Pacific (Galapagos) in (1) March–April, (2) September–October and (3) December, from (4) the central and western Pacific in March, and (5) from Brazil in November. Available soundings from multiple years in the same season and location were averaged together.

[13] Each profile is an average of 3–20 soundings. A 0.5 km width boxcar smoother is applied to all fields. The temperature above 20 km is blended into monthly mean profiles (zonal mean, but for each latitude) from United Kingdom Meteorological Office (UKMO) stratospheric analyses. Individual profile months and latitudes are used to construct UKMO average temperature profiles.

[14] Water vapor is determined by sonde relative humidity converted to specific humidity and Hygrometer frost point temperature converted to specific humidity, then averaged together where they exist for each sounding. In practice, the TTL layer is almost exclusively Hygrometer data. The soundings are averaged together for a given location and month. Above 20 km a monthly mean water vapor climatology from the HALogen Occultation Experiment (HALOE) on the Upper Atmosphere Research Satellite (UARS) is smoothly blended with the data starting at 20 km. HALOE data are taken from the updated climatology of *Randel et al.* [1998]. Individual sounding locations (latitude and longitude) and months are averaged to make an average HALOE profile, and then this is blended into the water vapor profile. As with temperature, smoothing is applied in the vertical.

[15] Ozone profiles are constructed similarly to water vapor. Ozonesonde profiles are averaged, HALOE Ozone climatological profiles are averaged at the same locations and times, and then these two are blended above 20 km. By 27 km, all the data are from the climatologies, but below 20 km, all data are from soundings.

[16] Other radiatively active trace species (CFC-11, CFC-12, N_2O, CH_4 and CO_2) distributions are 'late 1990s' averages from NOAA-CMDL data (available at http://www.cmdl.noaa.gov). These data are rounded to the nearest part per million, billion or trillion from data tables.

[17] The profile for the Galapagos March case is illustrated in Figure 1. The tropopause (cold point and lapse rate) is indicated, as well as the level of maximum convective influence defined by the minimum in the lapse rate of

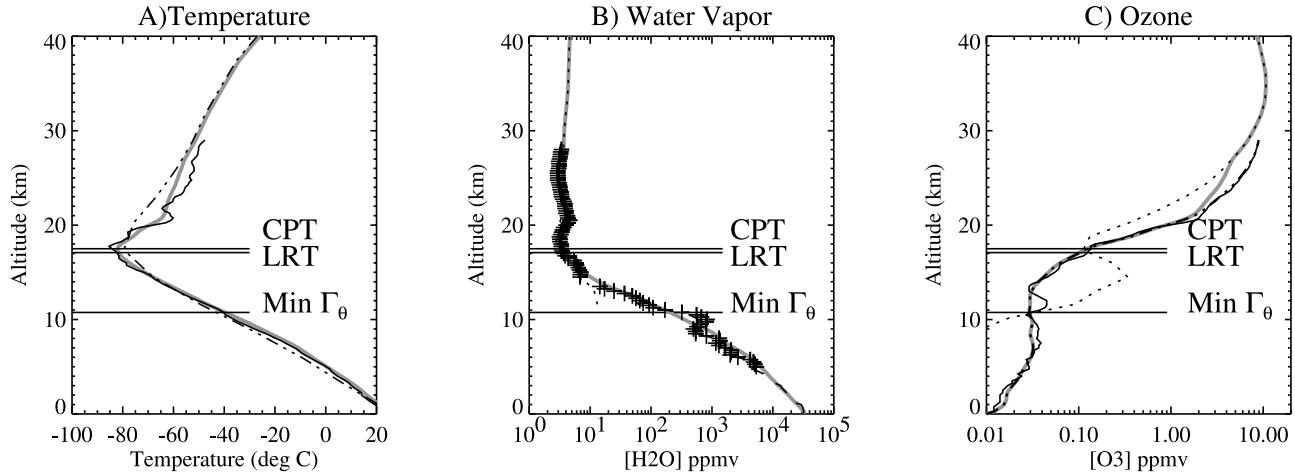


Figure 1. Profile for the Galapagos in March showing the merged profile input to the radiation calculations as a thick gray line in each panel. (a) Temperature. Individual radiosonde sounding temperature thin line, UKMO monthly mean temperature, 2-dot dashed. (b) Water vapor. An individual sounding humidity sensor dashed, and individual sounding frost-point hygrometer crosses. HALOE climatology dotted. (c) Ozone. An individual sounding from ozone sonde thin solid line, smoothed sounding 2 dot dash, HALOE ozone dotted. Solid horizontal lines indicate the altitude of the cold point tropopause (CPT), the lapse rate tropopause (LRT) and the minimum potential temperature lapse rate (Min Γ_θ).

potential temperature [*Gettelman and Forster*, 2002]. The March Galapagos profile in Figure 1 will be used as a standard to intercompare the radiation models. The four other profiles will be used for understanding variations in the radiation balance.

2.2. Models

[18] Five radiation models are used in this study. Two are detailed codes, two are codes for General Circulation Models (GCMs) and one is a Line-by-Line longwave code. This is not the first attempt to compare radiation codes in such a manner. Similar analyses (though not for the TTL explicitly) have been performed before, including the Intercomparison of Radiation Codes in Climate Models (ICRCCM) project [*Luther et al.*, 1988; *Ridgway et al.*, 1991].

[19] The National Center for Atmospheric Research (NCAR) Column Radiation Model (CRM) contains the same radiation codes as the atmospheric GCM in the NCAR Community Climate System Model (CCSM). In this study we have used two versions of the CRM. One contains the radiation codes from the Community Climate Model version 3 (CCM3) described by *Kiehl et al.* [1998]. The other is a version containing the radiation code from the newer Community Atmosphere Model version 2 (CAM2), described by *Collins et al.* [2002]. The radiation model uses a δ-Eddington shortwave scheme, and an absorptivity-emissivity longwave scheme [*Kiehl et al.*, 1996]. The major difference between the CAM2 and CCM3 codes is in the parameterization of the water vapor continuum (5–12 μm). The standard version (CRM-CCM3) contains the version of the continuum from *Roberts et al.* [1976], while the newer version (CRM-CAM2) contains a treatment of the continuum from the Clough, Kneizys and Davies model version 2.1 (CKD 2.1), based on *Clough et al.* [1989].

[20] The Center for Climate System Research (CCSR) Column model is also a radiation code optimized for a GCM. This model is incorporated in an atmospheric GCM developed at Center for Climate System Research and National Institute for Environmental Studies (CCSR/NIES) in Japan. The CCSR radiation code is based on the correlated *k*-distribution method with 13 bands (58 channels) in the shortwave and longwave radiation wavelengths [*Nakajima et al.*, 2000]. The water vapor continuum is treated using version 0 of the CKD model, developed by *Clough et al.* [1980].

[21] The Fu-Liou radiation scheme used in this study was originally developed by *Fu and Liou* [1992, 1993] with some modifications [*Rose and Charlock*, 2002]. The radiative transfer scheme is based on the delta-four-stream method for both solar and infrared spectra [*Liou et al.*, 1988; *Fu and Liou*, 1993] The correlated k-distribution method is used to treat the non-gray gaseous absorption due to H_2O, CO_2, O_3, N_2O, and CH_4 [*Fu and Liou*, 1992] with the addition of CFCs and CO_2 in the window region [*Kratz and Rose*, 1999]. The H_2O continuum absorption, CKD2.4 [*Tobin et al.*, 1999] is used in the whole thermal spectra (0–2850 cm^{-1}). The modifications affecting the solar radiation include an inclusion of O_2 and CO_2 absorption by means of a correction based on work by *Chou and Suarez* [1999] and an inclusion of minor absorption by H_2O in the visible.

[22] The Reading model is a detailed radiation code which uses a 10 cm^{-1} Narrow Band parameterization in the thermal infrared [*Shine*, 1991]. The version in this study employs the CKD 2.1 water vapor continuum and has updated gas absorption cross sections [*Forster and Shine*, 1997]. In the shortwave it uses a high resolution Discrete-Ordinate model for the ultraviolet and visible and a δ-Eddington model for water vapor absorption and scattering in the longwave. It has no shortwave carbon dioxide absorption.

[23] In addition we have also calculated the radiation balance for the standard profile using a Line by Line radiation code, the Reference Forward Model (RFM) [*Dudhia*, 1997] version 4.21. This is a line-by-line (LBL) radiative transfer model based on the GENLN2 model [*Edwards*, 1987]. It has been compared with other line by line models and validated against observations [*Sihra et al.*, 2001]. The treatment of the water vapor continuum in RFM is from the CKD model version 2.4.1 (CKD2.4.1), described by *Tobin et al.* [1999].

3. Results

[24] In this section we first describe input data profiles in the TTL (Section 3.1). We then detail the net radiation balance of the TTL and the role of individual gases in Section 3.2. In Section 3.3 we examine differences between the models. Section 3.4 focuses on the level of $Q_{clear} = 0$ and Section 3.5 examines the sensitivity of the radiation balance to radiatively active greenhouse gases and clouds.

3.1. Profile Data

[25] Figure 2 displays input data (of temperature, water vapor and ozone) for all five of the profiles used in the radiation calculations. Cold point tropopause temperatures (Figure 2a) vary from 189–198°K, coldest over the eastern Pacific in December and March; they are warmest (and lowest) in September in the eastern Pacific. This is consistent with the overall annual cycle of temperatures in the tropical tropopause region [*Holton et al.*, 1995]. The potential temperature of the tropopause is lowest (373 K) over the central and western Pacific in March, and highest (393 K) over Brazil in November.

[26] Of the 5 soundings, the minimum in TTL water vapor (Figure 2b) is lowest in the central and western Pacific in March (~2 ppmv) and the TTL minimum is highest over the Galapagos in September (~3 ppmv at 20 km, or 5 ppmv at the tropopause). The profiles are consistent with the stratospheric 'tape recorder' [*Mote et al.*, 1996] with higher water vapor in the July–September season persisting until November or December, and low water vapor from December through March.

[27] Ozone is illustrated in Figure 2c. The March profile in the central and western Pacific has significantly lower ozone in the TTL, likely due to the influence of deep convection and a clean boundary layer. Over the Galapagos, ozone is much higher in September than December or March, consistent with *Thompson et al.* [2003b].

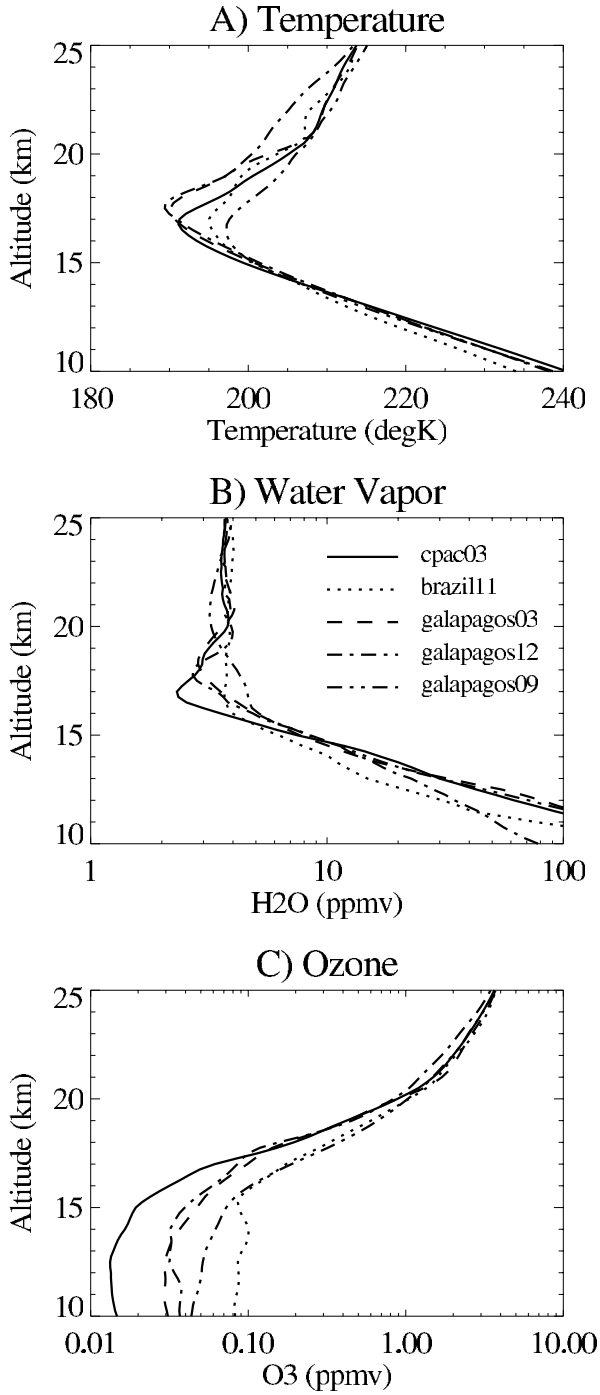


Figure 2. TTL profiles (from 10–25 km) of (a) temperature, (b) water vapor, and (c) ozone. March central and western Pacific solid, November Brazil dotted, March Galapagos dashed, December Galapagos dot-dash and September Galapagos 2 dot-dash.

3.2. Net Radiation and Individual Gas Contributions

[28] Figure 3 illustrates the radiative heating rate profile (Figure 3a), the net heating rates in the TTL (Figure 3b), and the components from various gases in the infrared (Figure 3c) all from the NCAR-CRM. The results are based on a calculation with a single diurnal average solar zenith angle. The overall radiative balance (Figure 3a) shows net radiative cooling due to longwave cooling in the troposphere, which changes in the TTL to a net radiative heating in the stratosphere, due to shortwave heating partially balanced by radiative cooling above 25 km.

[29] The level of $Q_{clear} = 0$ (Figure 3b) is located at about 15.1 km, about 2 km below the Lapse Rate Tropopause (LRT), and 2.5 km below the Cold Point Tropopause (CPT). The level is closer to the tropopause than to the minimum lapse rate of potential temperature (Min Γ_θ), marking the 'base' of the TTL and the level of maximum convective influence on the thermodynamic profile [*Gettelman and Forster*, 2002]. The location of $Q_{clear} = 0$ in other models and other profiles will be examined in more detail in Section 3.3.

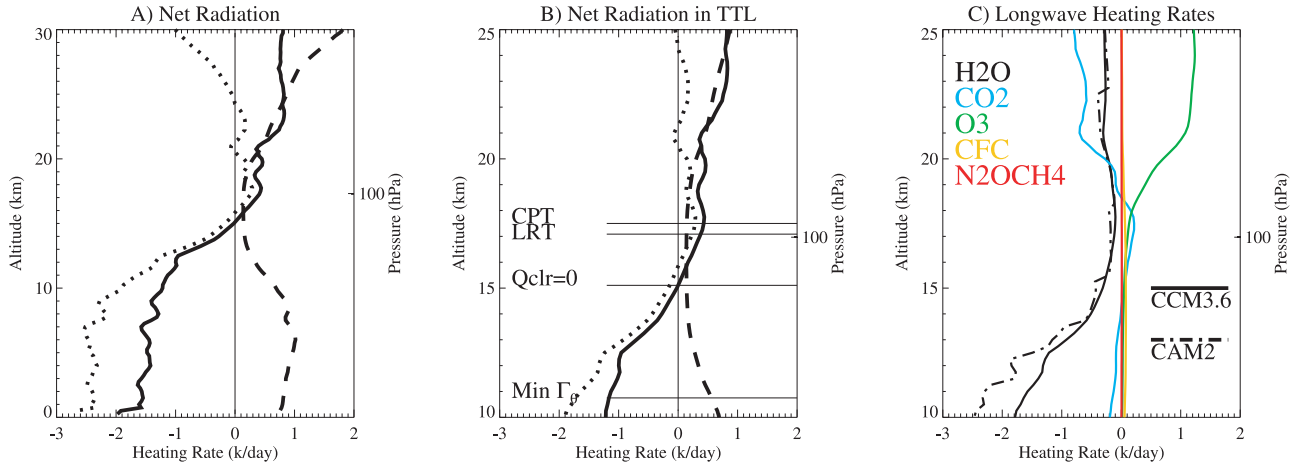


Figure 3. March Galapagos profiles showing diurnally averaged heating rates (in K day^{-1}) from the NCAR CRM (CCM3.6). (a) 0–30 km and (b) TTL (10–25 km). Shortwave (SW) dashed, Longwave (LW) dotted and Net solid. (c) Longwave (Infrared) heating rates broken down by gas for two versions of the NCAR-CRM as discussed in the text.

[30] Figure 3c breaks down the longwave or infrared heating rates by radiatively active species, and for two versions of the NCAR CRM. To determine heating rates for the 5 gases or groups of gases, the radiation model was run with all other radiatively active gases set to negligible (near-zero) values. Strictly speaking, these calculations are not truly independent. There are some differences between the longwave heating rates calculated as the sum of each gas (Figure 3c) and when all gases are included simultaneously (the dotted line in Figures 3a and 3b). This discrepancy is likely due to the dependence/overlap of a part of the H_2O rotation band with the CO_2 15μm band. Removing CO_2 influences the H_2O longwave cooling rate calculation by enhancing the transmission to space. Errors in the TTL are generally small, however, even in percentage terms. The discussion on a gas-by-gas basis is qualitative, and mostly for comparison purposes between models (which are affected the same way).

[31] In Figure 3c, the dominant cooling term is water vapor in the lower part of the TTL. The level of $Q_{clear} = 0$ is located near where the water vapor cooling is low. CO_2 has a small heating effect just around the tropopause, and then longwave heating from Ozone is partially balanced by smaller cooling from CO_2 and water vapor. The contributions to the net heating from chlorofluorocarbons (CFCs: CFC-11 and CFC-12) as well as from the sum of N_2O and CH_4 are negligible. As noted by *Thuburn and Craig* [2002] and *Hartmann and Larson* [2002], the reduction of the gross heating and cooling significantly lengthens the radiative damping time for temperature perturbations in the region between 14–18 km.

[32] Also shown in Figure 3c are calculations from the CAM2 version of the NCAR CRM model. All the gases are identical except for water vapor, which has a different treatment of the water vapor continuum near the water vapor rotational bands [*Collins et al.*, 2002]. This difference has a significant effect on the cooling in the model in the lower part of the TTL and the middle to lower troposphere, changing the longwave cooling by almost 40% at 10 km. The variations in the CAM2 model are due to the use of a

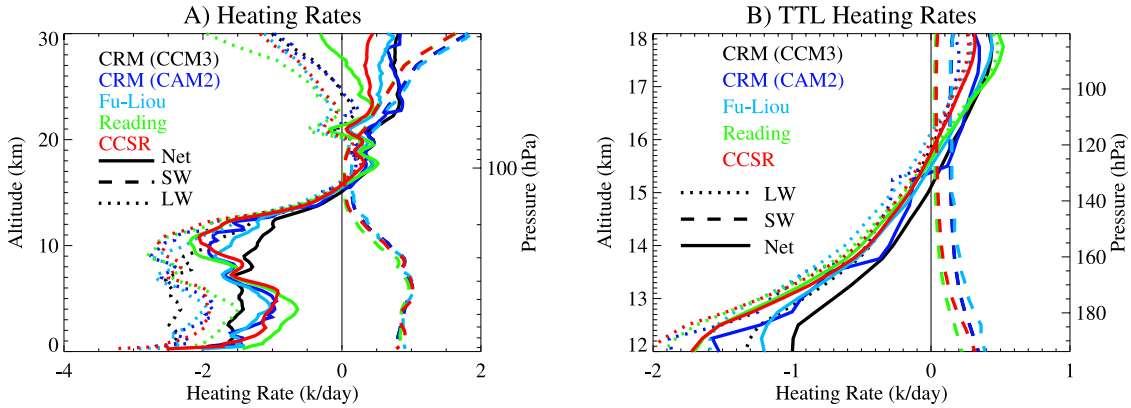


Figure 4. Profiles of Net (solid), Shortwave (SW- dashed) and Longwave or Infrared radiation (LW- dotted) from 5 different models. (a) Heating rates (in K day^{-1}) from 0–30 km. (b) Heating rates (in K day^{-1}) in the Tropical Tropopause Layer from 12–18 km. Individual models colored: NCAR CRM (CCM3 version) black, NCAR CRM (CAM2 version) dark blue, Fu-Liou light blue, Reading green and CCSR red.

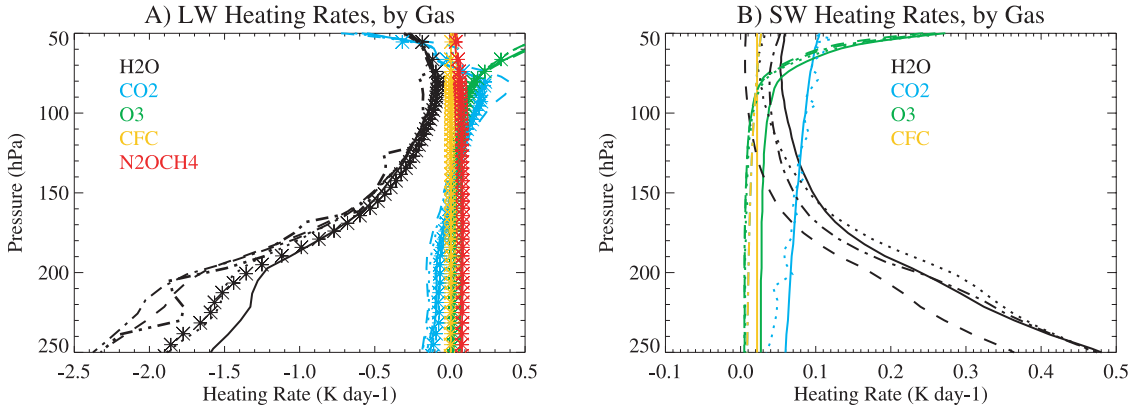


Figure 5. Heating rates (K day^{-1} for different models for (a) IR or Longwave and (b) Shortwave. Models: NCAR CRM (CCM3.6) solid, Reading dashed, Fu-Liou dotted and CCSR dot dash. In (a) only: NCAR CRM (CAM2) 2 dot dashed and Line by Line calculations asterisk. Gases are indicated by color: H_2O black, CO_2 light blue, O_3 green, CFCs yellow and N_2O + CH_4 red.

version of the code with a coarse lookup table, and have no geophysical significance.

3.3. Different Models

[33] The radiation balance of the atmosphere for the March Galapagos profile from 5 different models is illustrated in Figure 4. In this figure, as in Figure 3, the calculations represent diurnal averages calculated using an average solar zenith angle. In general, the models all show similar features. The Q_{clear} = 0 level, where net radiation changes sign from cooling to heating (with increasing altitude), is located near 15.5 km or around 130 hPa, as indicated in Figure 4b. The altitude of Q_{clear} = 0 varies over a range of ~500 m in the models, from about 15.1–15.7 km.

[34] From Figure 4a it is clear that the models have significant variation in their longwave cooling in the troposphere, which gives significant differences in the net radiation up to the TTL (12–14 km). The differences are probably due to different treatments of water vapor, to be discussed in more detail below.

[35] The short wave heating rates in the TTL also differ significantly, in two clusters. The CRM and Fu-Liou models have nearly twice the shortwave heating at 160 hPa (14 km) as the CCSR and Reading models. This difference will result in different sensitivities to changes in shortwave radiation over the diurnal cycle (see Section 3.4).

[36] The longwave and shortwave components for all the various models are compared in Figure 5. Five different model runs for the same average March Galapagos profile are shown, representing diurnal averages in the longwave (Figure 5a) and shortwave where available (Figure 5b). In addition, a calculation using a detailed line-by-line radiation code is shown in the Longwave (Figure 5a). In the Longwave (Figure 5a), there is generally good agreement between the models, except for major differences in water vapor. In addition, the Reading model indicates more CO_2 heating around the tropopause than the other models.

[37] The large differences in the longwave or infrared cooling from water vapor in Figure 5a are coherent. In general, the CCSR, CRM-CAM2 and Reading model cluster around one set of values for the H_2O cooling, while the Fu-Liou model lies very close to the line-by-line calculations and the CRM-CCM3 has less cooling than the other models. These differences are consistent with different versions of the water vapor 'continuum.' The CRM-CCM3 uses the *Roberts et al.* [1976] continuum. The CRM-CAM2 and Reading model use the CKD2.1 [*Clough et al.*, 1989] parameterization, while the Fu-Liou model and the RFM line-by-line calculations use the CKD2.4 parameterization [*Tobin et al.*, 1999], and the CCSR model uses the CKD0 parameterization [*Clough et al.*, 1980], which is very similar to CKD2.1. For further information on details of the CKD model versions as well as updates, see the documentation at http://www.rtweb.aer.com.

[38] These effects are even more pronounced in the troposphere below the TTL, and significantly impact the vertical distribution of net atmospheric cooling, as indicated in Figure 4a (especially note the difference between the otherwise identical CRM-CAM2 and CRM-CCM3). The impact of different versions of water vapor continuum absorption on climate have been noted in several studies using GCMs by *Iacono et al.* [2000], *Zhong and Haigh* [1999] and *Schwartzkopf and Ramaswamy* [1999], and the differences here are consistent with these studies. The continuum (5-12 μm) only affects the lower and mid troposphere. The rotational bands of water vapor (>20 μm) are important in the upper troposphere. The water vapor continuum effect on the upper troposphere radiative cooling rates is related to the water vapor foreign continuum.

[39] Figure 5b illustrates the components in the shortwave. Note that not all the models include all of the individual gases. In general there is good agreement in the shortwave, with the notable exception of significantly less shortwave heating from water vapor in the Reading model. In Figure 4b the total shortwave heating is less in the Reading and CCSR models. The Reading and CCSR models do not have shortwave CO_2 heating. This does not affect the mean level of Q_{clear} = 0 substantially (Figure 4b and Section 3.4 below), but it will have an impact as shortwave radiation varies.

[40] Figure 6 highlights some of the differences from the detailed line by line calculations. Five model runs are differenced from a line by line calculation with the same March Galapagos profile. The major differences from the

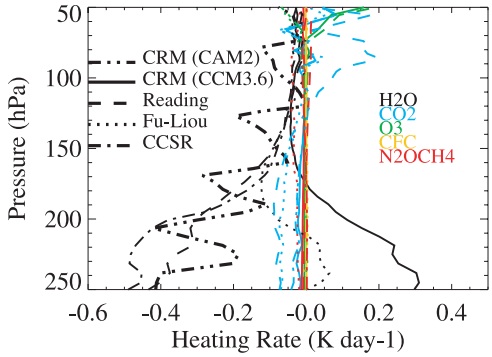


Figure 6. Difference from Line by Line Calculations for infrared heating rates in the Tropical Tropopause Layer, pressure scale. Models: NCAR CRM (CCM3.6) solid, Reading dashed, Fu-Liou dotted, CCSR dot dash and NCAR CRM (CAM2) 2 dot dash. Gases are indicated by color: H_2O black, CO_2 light blue, O_3 green, CFCs yellow and N_2O + CH_4 red.

line by line calculations are those indicated broadly above due to the different treatment of the water vapor continuum. Water vapor longwave cooling is larger in the CRM-CAM2, Reading and CCSR models which use CKD version 0 or version 2.1, and less H_2O cooling is found in the CRM-CCM3 model which uses *Roberts et al.* [1976]. The Fu-Liou model has similar cooling to the line-by-line calculations as both use CKD version 2.4. The oscillatory structure of the CRM-CAM2 model in Figure 6 is due to a coarse lookup table and has no geophysical significance. These differences become small near the level of $Q_{clear} = 0$. There are several anomalies in other gases. The Reading model has larger LW heating from CO_2 just around the tropopause from about 120–70 hPa, and more cooling from CO_2 below.

3.4. Level of Zero Net Heating

[41] With detailed information about the effects of gases and difference between models, we can proceed to examine in detail the level of $Q_{clear} = 0$ for the various models and profiles. Figure 7 shows the height, pressure, temperature and potential temperature of $Q_{clear} = 0$ for 4 different models and 5 different profiles. In addition to a calculation based on a daily average solar zenith angle for each location and each model, calculations are also illustrated for local solar noon. The Fu-Liou model also has been run using an exact diurnal cycle averaged together. For the standard Galapagos March profile, differences in the level of $Q_{clear} = 0$ between the diurnal average, and the average of profiles throughout the day are −0.2 km, 4.4 hPa and 1.2°K (with the daily average of multiple runs lower). This is not a significant difference from the values in Figure 7.

[42] The altitude of $Q_{clear} = 0$ is approximately 15.3 km among the 5 profiles, ranging from 15.0 to 15.6 km (Figure 7a). It is highest for the Galapagos in December, followed by the Galapagos in March. In September over the Galapagos $Q_{clear} = 0$ is found at 15 km. Corresponding pressures (Figure 7b) range from 132–118 hPa, with a similar distribution (lowest pressure in Galapagos in December, highest pressure over the Galapagos in September).

[43] The temperature of the location of $Q_{clear} = 0$ (Figure 7c) falls within a very tight band, an average across profiles of 198–201°K, with a spread across profiles of any one model about 3°K. Potential temperatures of the level of $Q_{clear} = 0$ (Figure 7d) range from 360–365 K. The profiles with higher altitude of $Q_{clear} = 0$ have slightly colder temperatures, but higher potential temperatures.

[44] It is quite interesting that the tropopause temperature among the profiles varies by 19°K (189–198°K) in Figure 7d, while the temperature of the level of $Q_{clear} = 0$ varies by only 3°K (Figure 7c). For some profiles, the temperature of $Q_{clear} = 0$ is quite close to the tropopause temperature because of the near isothermal nature of the TTL in September (Galapagos) and November (Brazil). The implication is that variations in $Q_{clear} = 0$ are not due to the tropopause structure. The logical explanation is that the water vapor cooling determines the location of $Q_{clear} = 0$ and that this is fixed in temperature because water vapor, the major contributor to the radiative balance, is also fixed in temperature [*Hartmann and Larson*, 2002]. However, we do not see the same range of observed variability in the pressure of $Q_{clear} = 0$ in the observations for a given range of Sea Surface Temperatures as predicted in a radiative-convective model by *Hartmann and Larson* [2002], likely because the real TTL is not in total radiative-convective equilibrium. So we are unable to conclusively validate the hypotheses of *Hartmann and Larson* [2002].

[45] Instantaneous balances for local noon were also calculated. For these cases, altitudes are 1–1.5 km lower (13.5–14 km) at pressures of ∼150 hPa, and temperatures are nearly 10°K warmer. Potential temperatures are also 5–8 K warmer. This indicates that there is a diurnal cycle to the level of $Q_{clear} = 0$. Closer to local noon, more radiative heating exists in the clear sky. For a given part of the TTL, this implies a range of altitudes at which net radiative heating begins.

[46] In general, there is good agreement between models, and similar variations are seen between different profiles. In Figure 7a, there are variations in $Q_{clear} = 0$ between models of about ±300 m in altitude. In general, the NCAR CRM is generally lower and the Reading model is generally higher. This partially explains earlier estimates, as the higher estimate for $Q_{clear} = 0$ by *Gettelman and Forster* [2002] was based on the Reading model, while the 15 km estimate by *Sherwood* [2000] was based on the NCAR CRM, and the 15 km estimate of *Folkins et al.* [1999] is based on the Fu-Liou model (albeit all with different input data). The Reading and CCSR models have very little diurnal variation compared to the CRM or the Fu-Liou model. This is likely due to the reduced shortwave heating around 150 hPa in these models (Figure 4b). The reduced heating is a consequence of a lack of shortwave CO_2 absorption, which is the largest term in the TTL (between 140–70 hPa) in the Fu-Liou model and the NCAR CRM (see Figure 5b).

[47] Finally, we note that Figure 7d also illustrates the levels of the upper boundary of the TTL (the cold point tropopause) and the lower boundary (the minimum potential temperature lapse rate), as defined by *Gettelman and Forster* [2002]. A higher and lower pressure tropopause generally corresponds with a higher level of $Q_{clear} = 0$ and a lower level of maximum convective outflow (Min Γ_θ).

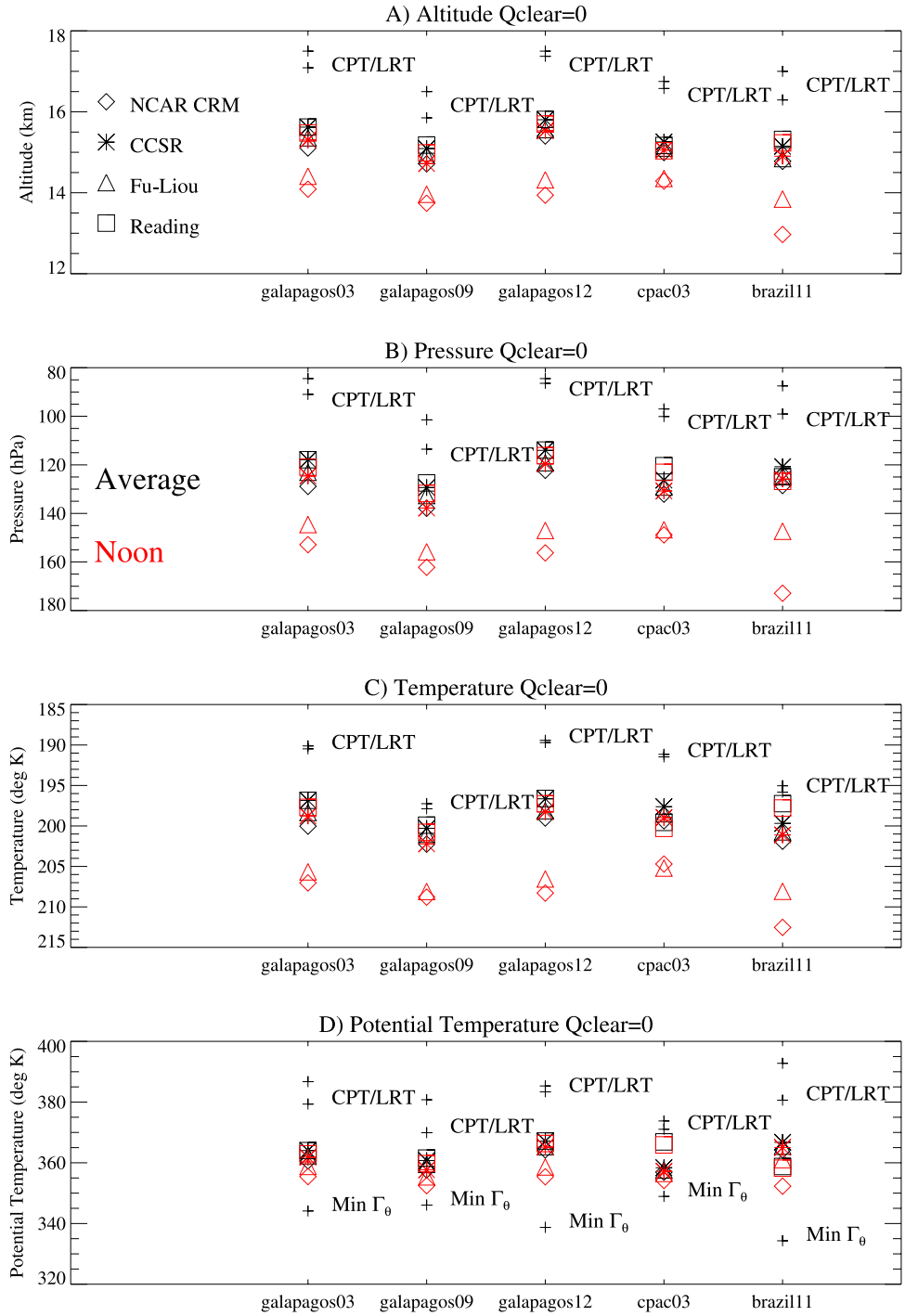


Figure 7. Level of zero clear sky radiative heating (Q_{clear} = 0) for 5 different profiles (X-axis). (a) Altitude (km), (b) pressure (hPa), (c) temperature (K) and (d) potential temperature (K). Models: CRM-CCM3 (diamonds), CCSR (asterisk) CCSR, Fu-Liou (triangles) and Reading (squares). Diurnal averages in black, noon values green. Cold Point Tropopause (CPT), Lapse Rate Tropopause (LRT) and the level of minimum θ lapse rate (Min Γ_θ) indicated by crosses. The CPT is always above the LRT.

[48] Fine scale vertical structures in the atmosphere also create local variations in the level of Q_{clear} = 0. Table 1 presents data for 24 individual profiles with continuous temperature, ozone and water vapor through the TTL, based on full (250 m) resolution and no smoothing. The altitude of Q_{clear} = 0 varies over nearly 1.5 km from the mean of a

Table 1. Anomalies of Q_{clear} = 0 in 24 Profiles

Metric, units	Minimum	Maximum	Std. Dev.
Altitude, km	−0.970	0.484	0.399
Pressure, hPa	−11.3	23.5	9.24
Temperature, °K	−3.02	5.39	2.56
Potential Temp, K	−7.73	7.10	3.45

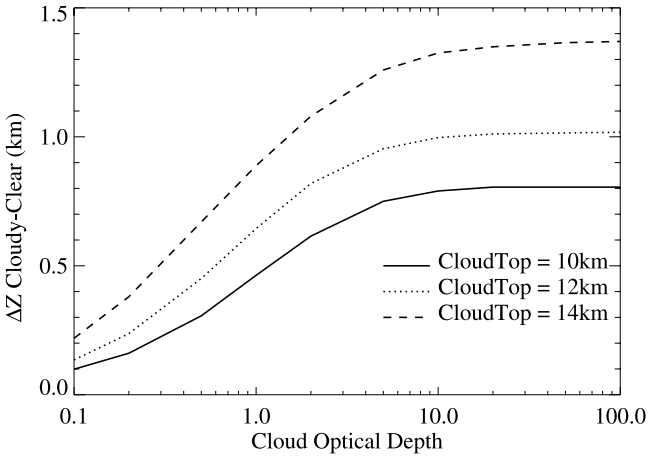


Figure 8. Change in altitude of $Q_{clear} = 0$ when clouds of different optical depths are inserted with a cloud top height of 10 km (solid), 12 km (dotted) and 14 km (dashed).

particular location and season, with a standard deviation of 400 m. Pressure varies over a range of 35 hPa, with a standard deviation of 9 hPa. The standard deviation of temperature is ~2.5°K, consistent with the height deviations, and that of potential temperature slightly larger (but not quite as large as would be expected from purely adiabatic adjustment to the temperature).

3.5. Sensitivity to GHGs and Clouds

[49] Finally, we briefly analyze potential changes to the level of $Q_{clear} = 0$ from changing radiatively active greenhouse gases and clouds. As illustrated in Figure 7c, the temperature of $Q_{clear} = 0$ remains at about 200°K for all of the conditions tested. We have performed several runs of the NCAR-CRM model and modified the important greenhouse gases (O_3, CO_2 and H_2O) to ascertain their effect on the radiation balance and the level of $Q_{clear} = 0$. Not surprisingly, increasing O_3 or CO_2 tends to lower the altitude of $Q_{clear} = 0$ by enhancing heating in the TTL, while increasing specific humidity (H_2O) tends to raise the level of $Q_{clear} = 0$ by enhancing the water vapor cooling (not shown). These variations are smaller than the inter profile or diurnal variations noted above. Since calculations with the column radiation models are made with fixed temperature profiles, it is hard to go beyond these general statements to understand all the potential feedbacks involved.

[50] A full treatment of the cloudy sky case is beyond the scope of this paper. However, we have performed sensitivity tests with two models (the Fu-Liou and NCAR-CRM models) to understand how clouds may modify the radiative balance. Figure 8 illustrates the effect of clouds on the radiation balance in the Fu-Liou model, using changes to the altitude of $Q_{clear} = 0$ as a diagnostic. The clouds are 4 km thick with cloud top heights of 10, 12 and 14 km and cloud optical depths ranging from 0.1 to 100. Most of the effect on the radiative balance occurs either above 18 km (80 hPa) or below the clouds, but there are defined changes in the TTL. The idealized thick high clouds in the TTL (cloud top heights of 10–14 km) in Figure 8 raise the level of $Q_{clear} = 0$ by up to 1–1.5 km, with an associated cooling of the level of $Q_{clear} = 0$ (not shown). Similar results are also found with the NCAR-CRM. The changes in the altitude of $Q_{clear} = 0$ occur due to increases in longwave cooling above the clouds. The change in cooling is more significant for thicker and higher clouds (though high clouds are usually thinner). The change is consistent with the cooling effects of clouds noted by other authors [*Doherty et al.*, 1984; *Sherwood*, 2000; *Hartmann et al.*, 2001]. The actual impact of clouds will depend on the cloud cover as well as the distribution of cloud optical depth and cloud top heights.

4. Radiation and Transport in the TTL

[51] The results of this study have several important implications for transport of air in the TTL, and into the stratosphere. Spatial gradients in the radiation balance, noted here as differences in the altitude of $Q_{clear} = 0$ between different locations in the tropics (Figure 7), indicate that air undergoing horizontal or near horizontal advection in the TTL may experience a range of heating rates, and even transit from regions of radiative heating to cooling along an isentropic surface, particularly if this surface is located between 355 and 370 K (potential temperature).

[52] Diurnal variations mean that parcels will actually see a spectrum of background insolation (and heating) over the course of a day. Because radiative damping timescales are long (~20–30 days in the TTL) the effect of diurnal variations may be small. However, for locations where the supply of moisture by convection may be locked to a diurnal cycle, the timing of convection may be important for the efficiency of lofting air after convective detrainment.

[53] Variations between individual profiles are caused by layered structures in the atmosphere, mostly layers of varying relative humidity [*Fujiwara et al.*, 2003]. Low humidity layers reduce the longwave cooling, and can lower the level of $Q_{clear} = 0$.

[54] All of these variations mean that air will experience a range of heating rates. The history of heating rates that an air mass experiences in its horizontal transport through the TTL may be important for understanding the origin of air into the stratosphere. For transport, the effect can be seen in the long residence times of air near this 'stagnation surface' noted by *Sherwood and Dessler* [2003] in a model with radiative heating and convection, and also in trajectory experiments by *Fueglistaler et al.* [2004].

[55] We also highlight the relationship between diabatic heating and convective transport. Clear sky parcels above $Q_{clear} = 0$ will rise into the stratosphere, and those below this level sink. According to Figure 7, the level of $Q_{clear} = 0$ is located around the 365 K potential temperature surface. According to *Folkins et al.* [2000], the level of the main outflow from deep convection (the most common level of a deep convective anvil) is centered around ~345 K (12–14 km). The level of $Q_{clear} = 0$ is thus located above the mode of the main convective outflow by 1–3 km. Because the level of $Q_{clear} = 0$ is above the level of the main convective outflow, only deeper convective events, those with cloud top temperatures and anvils colder than 200°K, will be able to supply air to the stratosphere, as air detraining below this level will sink once it leaves the anvil.

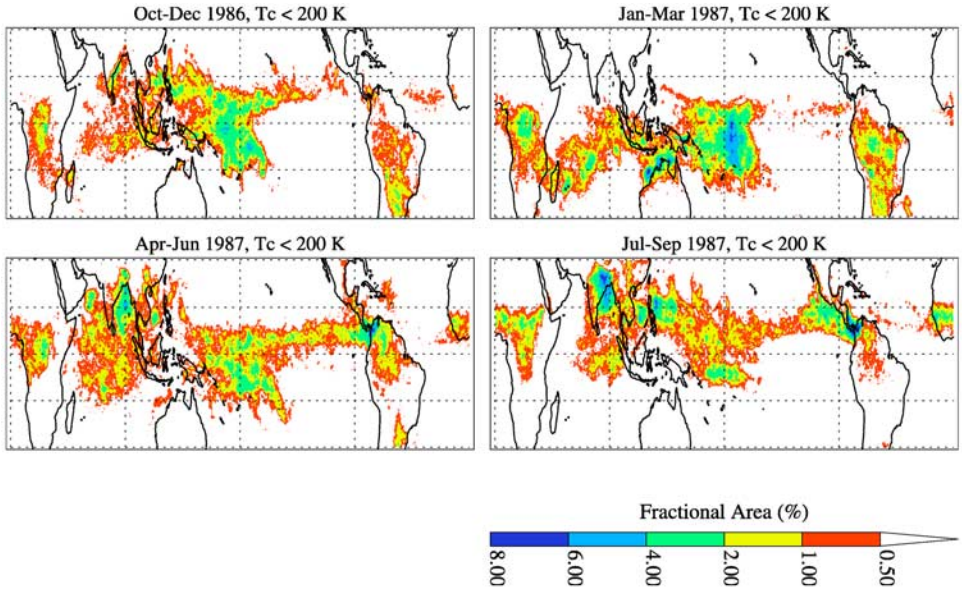


Figure 9. Fractional area coverage (or frequency) of observed convection observed colder than 200°K for four seasons during 1986–1987, in percent. October–December (upper left), January–March (upper right), April–June (lower right) and July–September (lower left).

[56] The locations where this convection occurs can be determined from satellite observations. Figure 9, based on the work of *Gettelman et al.* [2002], illustrates the location of cloud brightness temperatures colder than 200°K. There are several regions where cloud top brightness temperatures colder than 200°K are found more frequently, notably over the western Pacific from January–March (Figure 9b), over the Panama Bight from July–September (Figure 9d), and over the Ganges river valley during the South Asian summer monsoon from July–September (Figure 9d). Note that these events in the 'upper TTL', even in active regions, are episodic and are generally observed only about 5% of the time.

5. Conclusions

[57] We have examined in detail the radiation balance of several tropical profiles with varying temperatures, tropopause structures, water vapor and ozone. We have used four different radiation models (one with two versions) and a detailed line by line radiation code. The basic conclusions from this work are as follows:

[58] 1. Radiation models generally agree quite well in the TTL. The level of $Q_{clear} = 0$ may vary by ±300 m between models. This is nearly as much as the time and space variability, or sensitivity to radiatively active gases. Simplified codes for GCMs do not appear to be substantially different from detailed codes. Differences between models are due to two factors. First, differences in the absorption of solar radiation, particularly from CO_2 (1.4–2.7 μm band) which affects the TTL and determines sensitivity to the diurnal cycle. Two models (CCSR and Reading) have less shortwave absorption in the TTL (Figure 4b) because they do not include the shortwave effects of CO_2.

[59] Second, differences between models are due to the treatment of the water vapor continuum which affects heating rates in the lower and mid troposphere. The treatment of water vapor is critically important for climate below the TTL. Several authors have examined these impacts, including *Collins et al.* [2002] and *Iacono et al.* [2000] using the NCAR CCM3. Changes in heating and cooling may strongly influence the lower regions of the TTL near the level of main convective outflow, as well as affecting the outflow itself. This is easy to see in the differences between models throughout the troposphere (Figure 4a), and particularly the differences between the two versions of the NCAR-CRM, which are identical except for the treatment of water vapor continuum absorption.

[60] 2. The level of $Q_{clear} = 0$ is located at ~15 km, 125 hPa, 200°K and 360 K (potential temperature), in agreement with previous work. The water vapor distribution, which is affected by temperature, determines the level of $Q_{clear} = 0$. O_3 and CO_2 act to heat the TTL and lower the level of $Q_{clear} = 0$. The level of $Q_{clear} = 0$ appears to be nearly constant in temperature, consistent with *Hartmann and Larson* [2002], though observations do not show the same range of height or pressure variability with Sea Surface Temperature as a radiative–convective model.

[61] Longwave cooling from water vapor is dominant in the troposphere and tails off as the level of $Q_{clear} = 0$ is approached. Around this level, there is longwave and shortwave heating from CO_2 (Figure 5). Shortwave heating from O_3 begins above the TTL (60–50 hPa). The location of $Q_{clear} = 0$ is then a balance between H_2O, CO_2 and O_3.

[62] 3. There is some variability in the level of $Q_{clear} = 0$: ±300 m between models, ±500 m between different locations and seasons, ±400 m for individual profiles. Variability is substantial, up to ~1.5 km, for low solar zenith angles in the models which include shortwave absorption from CO_2 (NCAR-CRM and Fu-Liou). Given the variations in the background radiative heating field spatially and temporally, the radiative heating or cooling experienced by a parcel may vary significantly due to layers with large variations in humidity in the TTL.

[63] 4. The level of zero radiative heating is sensitive to greenhouse gas concentrations and to clouds. Increases in TTL ozone lower the level of $Q_{clear} = 0$ by enhancing absorption and heating. Changes in CO_2 alone also enhance absorption and lower the level of $Q_{clear} = 0$, but less than changes in O_3. Increases in water vapor tend to increase the altitude of $Q_{clear} = 0$, and slightly increase the temperature at which $Q_{clear} = 0$ (the rising altitude partially offsets cooler temperatures at higher altitudes). The presence of high clouds tends to increase longwave cooling above the clouds, which raises the altitude of $Q_{clear} = 0$ by as much as 1 km for opaque clouds at 12–14 km. The effect is more prominent for higher and thicker clouds.

[64] 5. The level of $Q_{clear} = 0$ is located above the level of main convective outflow by 1–3 km. Deeper convection would likely tend to moisten the TTL, and this would raise the level of $Q_{clear} = 0$ (higher and colder tropopause heights in Figure 7 are associated with a higher level of $Q_{clear} = 0$). In addition, upper tropospheric clouds increase the longwave cooling above them, and also tend to increase the level of zero net radiative heating. Thus the level of zero net radiative heating is likely to remain well above the outflow from most convection.

[65] 6. Convection needs to reach above the level of main convective outflow to loft air into a region of background heating where it can rise into the stratosphere. These regions are actually isolated in time and space. This might have a significant affect on the supply of humidity and trace species to the stratosphere, if climate changes affect the spatial distribution of the deepest convection. We may even conclude that there are specific 'Fountain' regions [after *Newell and Gould-Stewart*, 1981] for supplying air in the TTL above the level of $Q_{clear} = 0$ where it may rise into the stratosphere, and that stratospheric humidity may be acutely sensitive to these locations.

[66] Future work will attempt to propagate the lessons learned in this study into these radiation codes. We also plan to examine further the case of cloudy skies, and how radiative heating reacts with deep and shallow cloud fields in the tropics.

[67] **Acknowledgments.** We thank the Soundings of Ozone and Water in the Equatorial Region (SOWER) project for the use of sounding data taken at the Galapagos Islands. We also thank J. McCaa of NCAR for assistance with the CAM2 version of the NCAR-CRM. L. K. Gohar is supported by grant NER/L/S/2001/00661. The National Center for Atmospheric Research is supported by the U.S. National Science Foundation.

References

Brewer, A. W. (1949), Evidence for a world circulation provided by the measurements of helium and water vapor distribution in the stratosphere, *Q. J. R. Meteorol. Soc.*, *75*, 351–363.

Chou, M., and M. Suarez (1999), A solar radiation parameterization for atmospheric studies, *Tech. Rep., NASA/TM-1999-104606*, 40 pp.

Clough, S. A., F. X. Kneizys, R. W. Davies, R. Gamache, and R. H. Tipping (1980), *Theoretical Line Shape for H_2O Vapor: Application to the Continuum*, Academic, San Diego, Calif.

Clough, S. A., F. X. Kneizys, and R. W. Davies (1989), Line shape and the water vapor continuum, *Atmos. Res.*, *23*, 229–241.

Collins, W. D., J. K. Hackney, and D. P. Edwards (2002), An updated parameterization for infrared emission and absorption by water vapor in the National Center for Atmospheric Research Community Atmosphere Model, *J. Geophys. Res.*, *107*(D22), 4664, doi:10.1029/2001JD001365.

Doherty, G. M., R. E. Newell, and E. F. Danielsen (1984), Radiative heating rates near the stratospheric fountain, *J. Geophys. Res.*, *89*(D1), 1380–1384.

Dudhia, A. (1997), Rfm v3 software user's manual, *Tech. Rep. ESA Doc. PO-MA-OXF-GS-0003*, Dep. of Atmos., Oceanic, and Planet, Phys., Univ. of Oxford, Oxford, UK.

Edwards, D. (1987), GENLN2: The new oxford line-by-line atmospheric transmittance/radiance model: Description and user's guide, *Tech. Rep. 87.2*, Dep. of Atmos., Oceanic, and Planet. Phys., Univ. of Oxford, Oxford, UK.

Folkins, I., M. Loewenstein, J. Podolske, S. J. Oltmans, and M. Proffitt (1999), A barrier to vertical mixing at 14 km in the tropics: Evidence from ozonesondes and aircraft measurements, *J. Geophys. Res.*, *104*(D18), 22,095–22,102.

Folkins, I., S. J. Oltmans, and A. M. Thompson (2000), Tropical convective outflow and near-surface equivalent potential temperatures, *Geophys. Res. Lett.*, *27*(16), 2549–2552.

Forster, P. M. de F., and K. P. Shine (1997), Radiative forcing and temperature trends from stratospheric ozone depletion, *J. Geophys. Res.*, *102*, 10,841–10,855.

Fu, Q., and K. Liou (1992), On the correlated k-distribution method for radiative transfer in nonhomogeneous atmosphere, *J. Atmos. Sci.*, *49*, 2139–2156.

Fu, Q., and K. Liou (1993), Parameterization of the radiative properties of cirrus clouds, *J. Atmos. Sci.*, *50*, 2008–2025.

Fueglistaler, S., H. Wernli, and T. Peter (2004), Tropical troposphere-to-stratosphere transport inferred from trajectory calculations, *J. Geophys. Res.*, *109*, D03108, doi:10.1029/2003JD004069.

Fujiwara, M., F. Hasebe, M. Shiotani, N. Nishi, H. Vömel, and S. J. Oltmans (2001), Water vapor control at the tropopause by equatorial Kelvin waves observed over the Galapagos, *Geophys. Res. Lett.*, *28*(16), 3143–3146.

Fujiwara, M., S.-P. Xie, M. Shiotani, H. Hashizume, F. Hasebe, H. Vömel, S. J. Oltmans, and T. Watanabe (2003), Upper tropospheric inversion and easterly jet in the tropics, *J. Geophys. Res.*, *108*(D24), 2796, doi:10.1029/2003JD003928.

Gettelman, A., and P. M. de F. Forster (2002), A climatology of the tropical tropopause layer, *J. Meteorol. Soc. Jpn.*, *80*(4B), 911–924.

Gettelman, A., M. L. Salby, and F. Sassi (2002), The distribution and influence of convection in the tropical tropopause region, *J. Geophys. Res.*, *107*(D10), 4080, doi:10.1029/2001JD001048.

Hartmann, D. L., and K. Larson (2002), An important constraint on tropical cloud-climate feedback, *Geophys. Res. Lett.*, *29*(20), 1951, doi:10.1029/2002GL015835.

Hartmann, D. L., J. R. Holton, and Q. Fu (2001), The heat balance of the tropical tropopause, cirrus, and stratospheric dehydration, *Geophys. Res. Lett.*, *28*, 1969–1972.

Highwood, E. J., and B. J. Hoskins (1998), The tropical tropopause, *Q. J. R. Meteorol. Soc.*, *124*(549), 1579–1604.

Holton, J. R., and A. Gettelman (2001), Horizontal transport and dehydration in the stratosphere, *Geophys. Res. Lett.*, *28*(14), 2799–2802.

Holton, J. R., P. H. Haynes, A. R. Douglass, R. B. Rood, and L. Pfister (1995), Stratosphere-troposphere exchange, *Rev. Geophys.*, *33*(4), 403–439.

Iacono, M. J., E. J. Mlawer, S. A. Clough, and J.-J. Morcrette (2000), Impact of an improved longwave radiation model, RRTM, on the energy budget and thermodynamic properties of the NCAR community climate model, CCM3, *J. Geophys. Res.*, *105*(D11), 14,873–14,890.

Kiehl, J. T., J. J. Hack, G. B. Bonhan, B. A. Boville, B. P. Briegleb, D. L. Williamson, and P. J. Rasch (1996), Description of the NCAR community climate model (CCM3), *Tech. Rep. 420*, Natl. Cent. for Atmos. Res., Boulder, Colo.

Kiehl, J. T., J. J. Hack, G. B. Bonan, B. A. Boville, D. L. Williamson, and P. J. Rasch (1998), The National Center for Atmospheric Research Community Climate Model: CCM3, *J. Clim.*, *11*(6), 1131–1149.

Kratz, D., and F. Rose (1999), Accounting for molecular absorption within the spectral range of the CERES window channel, *J. Quant. Spectrosc. Radiat. Transfer*, *48*, 83–95.

Liou, K., Q. Fu, and T. Ackerman (1988), A simple formulation of the delta-four-stream approximation for radiative transfer parameterizations, *J. Atmos. Sci.*, *45*, 1940–1947.

Luther, F. M., R. G. Ellingson, Y. Fouquart, S. Fels, N. A. Scott, and W. J. Wiscombe (1988), Intercomparison of Radiation Codes in Climate Models (ICRCCM): Longwave clear-sky results—A workshop summary, *Bull. Am. Meteorol. Soc.*, *69*(1), 40–48.

Mote, P. W., et al. (1996), An atmospheric tape recorder: The imprint of tropical tropopause temperatures on stratospheric water vapor, *J. Geophys. Res.*, *101*(D2), 3989–4006.

Nakajima, T., M. Tsukamoto, Y. Tsushima, A. Numaguti, and T. Kimura (2000), Modeling of the radiative processes in an atmospheric general circulation model, *Appl. Opt.*, *39*, 4869–4878.

Newell, R. E., and S. Gould-Stewart (1981), A stratospheric fountain?, *J. Atmos. Sci.*, *38*, 2789–2796.

Oltmans, S. J., H. Vömel, D. J. Hofmann, K. H. Rosenlof, and D. Kley (2000), The increase in stratospheric water vapor from balloon-borne, frostpoint hygrometer measurements at Washington, D.C. and Boulder, Colorado, *Geophys. Res. Lett.*, *27*(21), 3453–3456.

Randel, W. J., F. Wu, J. M. Russell III, A. Roche, and J. W. Waters (1998), Seasonal cycles and QBO variations in stratospheric CH_4 and H_2O observed in UARS HALOE data, *J. Atmos. Sci.*, *55*(2), 163–185.

Ridgway, W. L., S. Harshvardhan, and A. Arking (1991), Computation of atmospheric cooling rates by exact and approximate methods, *J. Geophys. Res.*, *96*(D5), 8969–8984.

Roberts, R. E., J. E. A. Salby, and L. M. Biberman (1976), Infrared continuum absorption by atmospheric water vapor in the 8–12 μm window, *Appl. Opt.*, *15*, 2085–2090.

Rose, F., and T. Charlock (2002), New Fu-Liou code tested with ARM Raman lidar and CERES in pre-CALIPSO exercise, paper presented at 11th Conference on Atmospheric Radiation, Am. Meteorol. Soc., Ogden, Utah.

Schwartzkopf, M. D., and V. Ramaswamy (1999), Radiative effects of CH_4, N_2O, halocarbons and the foreign-broadened H_2O continuum: A GCM experiment, *J. Geophys. Res.*, *104*(D8), 9467–9488.

Sherwood, S. C. (2000), A stratospheric "drain" over the maritime continent, *Geophys. Res. Lett.*, *27*(5), 677–680.

Sherwood, S. C., and A. E. Dessler (2003), Convective mixing near the tropopause: Insights from seasonal variations, *J. Atmos. Sci.*, *60*(22), 2674–2685.

Shine, K. P. (1991), On the relative greenhouse strength of gases such as the halocarbons, *J. Atmos. Sci.*, *48*, 1513–1518.

Sihra, K., M. D. Hurley, K. P. Shine, and T. J. Wallington (2001), Updated radiative forcing estimates of 65 halocarbons and nonmethane hydrocarbons, *J. Geophys. Res.*, *106*, 20,493–20,505.

Stratospheric Processes and Their Role in Climate (SPARC) (2000), Assessment of water vapor in the upper troposphere and lower stratosphere, *Tech. Doc. WMO/TD-1043*, World Meteorol. Org., Paris.

Thompson, A. M., et al. (2003a), The 1998–2000 SHADOZ tropical ozone climatology: 1. Comparison with TOMS and ground-based measurements, *J. Geophys. Res.*, *108*(D2), 8238, doi:10.1029/2001JD000967.

Thompson, A. M., et al. (2003b), The 1998–2000 SHADOZ tropical ozone climatology: 2. Tropospheric variability and the zonal wave-one, *J. Geophys. Res.*, *108*(D2), 8241, doi:10.1029/2002JD002241.

Thuburn, J., and G. C. Craig (2002), On the temperature structure of the tropical substratosphere, *J. Geophys. Res.*, *107*(D2), 4017, doi:10.1029/2001JD000448.

Tobin, D., et al. (1999), Downwelling spectral radiance observations at the Sheba ice station: Water vapor continuum measurements from 17 to 26 μm, *J. Geophys. Res.*, *104*, 2081–2092.

Vömel, H., et al. (2002), Balloon-borne observations of water vapor and ozone in the tropical upper troposphere and lower stratosphere, *J. Geophys. Res.*, *107*(D14), 4210, doi:10.1029/2001JD000707.

Zhong, W., and J. D. Haigh (1999), The sensitivity of long-wave radiation fields and the response of a GCM to water-vapour continuum absorption, *Q. J. R. Meteorol. Soc.*, *125*, 1383–1406.

M. Ammerman, Q. Fu, and C. Johanson, Department of Atmospheric Sciences, University of Washington, Seattle, WA 98195, USA.

P. M. de F. Forster and L. K. Gohar, Department of Meteorology, University of Reading, Reading RG6 2AH, UK.

M. Fujiwara, Graduate School of Environmental Earth Science, Hokkaido University, 060-0810 Sapporo, Japan.

A. Gettelman, National Center for Atmospheric Research, Box 3000, Boulder, CO 80307-3000, USA. (andrew@ucar.edu)

H. Vömel, Climate Monitoring and Diagnostics Laboratory, National Oceanic and Atmospheric Administration, Boulder, CO 80303, USA.